

Raman-scattering study of photoexcited plasma in semiconducting and semi-insulating InP

R. Cuscó, J. Ibáñez, and L. Artús

Institut Jaume Almera, Consell Superior d'Investigacions Científiques (CSIC), Lluís Solé i Sabarís s.n., 08028 Barcelona, Spain

(Received 24 November 1997)

Raman scattering is used to study the photoexcited electron-hole plasma generated under continuous-wave laser excitation in semiconducting and semi-insulating InP at room temperature and at 80 K. Coupled plasmon-LO-phonon modes are detected in both types of samples, even at low laser excitation power. The coupled modes are clearly resolved from the depletion-zone LO mode in high-resolution measurements. This makes possible the accurate determination of the frequency and width of the unscreened LO-phonon peak. The photoexcited-plasma density is obtained for different incident laser powers by fitting the Raman spectra with a line-shape calculation based on a Lindhard-Mermin dielectric function that takes into account electron and hole contributions. [S0163-1829(98)12719-4]

I. INTRODUCTION

There is an increasing interest in InP because its electronic properties and excellent lattice match with low-band-gap alloys such as GaInAs, GaInAsP, AlInAs, and AlGaInAs make it attractive for applications in a wide range of electronic and optoelectronic devices. Thus, InP-based high-speed logic circuits that take advantage of the high electron mobility in InP have been reported.¹ Millimeter-wave sources and amplifiers based on InP are expected to operate at higher frequencies with lower noise and higher efficiency than those based on GaAs because of the larger separation between the Γ and L conduction-band minima.² p -type InP has also found use in the fabrication of high-efficiency Schottky-barrier solar cells.³ InP-based devices are also very suitable in applications for optical fiber communications, as they can operate in the low-loss window of silica fibers. Avalanche photodiodes based on the lattice matched GaInAsP/InP (Ref. 4) and GaInAs/InP (Ref. 5) systems have been reported to yield high quantum efficiency and fast response time in the 1.0–1.6- μm wavelength region. InP is a material very well suited to be used as a substrate for the fabrication of such devices. A good knowledge of the physical properties of InP, and in particular of the generation and dynamics of photoexcited charge, may offer valuable insights for the development of high-performance optoelectronic devices.

In this paper, we have used Raman scattering to study the electron-hole plasma generated by continuous-wave (cw) laser excitation in semiconducting and semi-insulating InP. The first observation of light scattering by photoexcited LO-plasmon coupled modes (LOPCM's) in a III-V semiconductor was reported in GaP excited with a high-power pulsed dye laser.⁶ Subsequently, extensive studies of light scattering by single-particle and collective excitations of the electron-hole plasma have been carried out, mainly on GaAs.⁷ By contrast, only a few studies have been reported so far on InP. The first experiments on light scattering by a photoexcited plasma in undoped InP, carried out using a two-photon absorption technique,⁸ showed small broadenings of the LO peak when high power densities of the pulsed laser were employed. In a later work, the time evolution of a nonequilibrium electron-hole plasma was studied in semi-insulating

InP by means of time-resolved Raman spectroscopy using separate pump and probe beams.⁹ At high exciting power densities ($\approx 10^3 \text{ W cm}^{-2}$) the LOPCM peak was unambiguously detected, and the photoexcited-plasma density was determined at different pump-probe delay times by fitting theoretical line shapes calculated from a Lindhard-Mermin dielectric function. A similar study was also carried out in n -type InP (Ref. 10), where the diffusion of the nonequilibrium plasma was analyzed in terms of a modified diffusion equation including a drift term.

The first observation of light scattering by LOPCM's in semiconducting InP under cw-laser excitation was reported by Nakamura and Katoda.¹¹ In lightly doped n -type InP, they observed a frequency shift to higher energies of the LOPCM peak when the laser-power density was increased from 10^2 to $1.2 \times 10^3 \text{ W cm}^{-2}$. Subsequent measurements performed on semiconducting InP in steady-state conditions¹² have clearly resolved the L^+ branch of the LOPCM's from the unscreened LO modes arising from the surface depletion zone, but only in spectra obtained with high power densities. However, the same authors could not resolve the L^+ peak from the LO peak in semi-insulating InP. Recently, polarized Raman-scattering measurements on a MOCVD-grown epitaxial layer of InP have been published.¹³ These results appear to be in conflict with previous data,^{11,12} as L^+ shifts of only 0.2 cm^{-1} are reported for large variations of laser power, in contrast with L^+ shifts of 15 cm^{-1} (Ref. 12) and 20 cm^{-1} (least doped sample of Ref. 11) found in previous works for lower laser-power densities.

For GaAs, light scattering by collective excitations of a photoexcited plasma in steady-state conditions could only be observed when the GaAs layers were buried between confining $\text{Al}_x\text{Ga}_{1-x}\text{As}$ layers.¹⁴ The fact that the photoexcited L^+ peak can be unambiguously observed from GaAs layers sandwiched between $\text{Al}_x\text{Ga}_{1-x}\text{As}$ layers, and not from bare GaAs surfaces, has been attributed to the high surface recombination velocity (SRV) at free GaAs surfaces,¹⁵ which is substantially reduced at the $\text{Al}_x\text{Ga}_{1-x}\text{As}/\text{GaAs}$ interface. The situation is quite different for InP. The low values of SRV for InP (Refs. 16–18) may explain the fact that it is possible to observe Raman scattering by LOPCM's from a bulk InP sample under cw-excitation conditions.

Light scattering by photoexcited LOPCM's has been reported in semi-insulating InP only under excitation with high-power laser pulses.^{9,15} Therefore, one might be inclined to believe that Raman spectra of semi-insulating InP obtained using cw-laser excitation at moderate powers are unaffected by photoexcited plasma, and, consequently, independent of the laser power used. In this paper, we present a light-scattering study of the electron-hole plasma generated by cw-laser excitation in semiconducting and semi-insulating InP in which we show that LOPCM's are detected in semi-insulating as well as in semiconducting InP, even at very low laser-power density. To our knowledge, this is the first time that light scattering by photoexcited LOPCM's has been reported in semi-insulating InP under cw-laser excitation. We study the photoexcited plasma as a function of the exciting laser power, at room temperature and at 80 K. The photoexcited-plasma density is extracted from the Raman spectra by fitting line-shape calculations based on a Lindhard-Mermin dielectric function that takes into account electron and hole contributions. Although some authors¹³ have neglected the hole contributions in previous Raman-scattering determinations of the photoexcited-plasma density, we show that neglecting the hole terms in the susceptibility leads to an overestimation of the plasma density. The line-shape fits to the measured Raman spectra have allowed us to compare the different plasma densities generated in semiconducting and semi-insulating InP at the same excitation level.

II. EXPERIMENT

In this work we have used (100)-oriented wafers of InP grown by the liquid-encapsulated Czochralski (LEC) method. The nominally undoped, semiconducting InP wafers were grown by MCP Wafer Technologies, Ltd. The electron concentration in these wafers was in the $(4.2\text{--}6.0) \times 10^{15} \text{ cm}^{-3}$ range, and the resistivity in the $0.31\text{--}0.22 \ \Omega \text{ cm}$ range. The Fe-doped, semi-insulating InP wafers were grown by Sumitomo using a LEC method in a phosphorus-controlled vapor pressure to reduce the dislocation density. Fe concentration in these wafers was in the $(1.6\text{--}4.2) \times 10^{16} \text{ cm}^{-3}$ range, and the resistivity in the $(1.2\text{--}4.2) \times 10^7 \ \Omega \text{ cm}$ range. The 528.7-nm line of an argon-ion laser was used as an excitation source. The Raman spectra were recorded using a T64000 Jobin-Yvon spectrometer equipped with a charge-coupled device detector cooled with liquid nitrogen. The polarized Raman measurements were carried out in the $z(x,y)\bar{z}$ scattering geometry. The experiments were performed using the triple additive configuration of the spectrometer with $100\text{-}\mu\text{m}$ slits. For this configuration, we have determined the spectral bandwidth to be $\approx 0.7 \text{ cm}^{-1}$ by deconvolving the first-order phonon peak of Si, measured at 80 K, with a triangular response function. The low-temperature measurements were carried out in a TBT liquid nitrogen cryostat.

The laser beam was focused to an elliptical spot of about $185 \times 285 \ \mu\text{m}^2$. The exciting laser powers were measured at the sample location, and we used values ranging from 3 to 55 mW, corresponding to power densities between 7 and 133 W cm^{-2} . For the low-temperature measurements the laser

power was adjusted to take into account the absorption of the cryostat windows.

III. THEORY: CALCULATION OF LOPCM LINE SHAPES

The theory of LOPCM's has long been well established for the coupling of LO phonons with the free-electron plasma in n -type semiconductors.⁷ For photoexcited electron-hole plasma in GaAs, it was observed that the two-component nature of the plasma modifies the spectra of the coupled modes, and intra- and inter-valence-band contributions to the susceptibility had to be included in the calculations.¹⁴ An extension of the LOPCM theory of Hon and Faust¹⁹ was proposed to deal with the coupling of LO modes with free-hole plasma,²⁰ in which the contributions to the susceptibility from intraband and interband transitions between degenerate spin- $\frac{3}{2}$ -like heavy- and spin- $\frac{1}{2}$ -like light-hole bands were taken into account. This theory has been used to model time-resolved Raman-scattering experiments carried out in photoexcited plasma in InP.⁹ Although the hole contribution to the susceptibility was not considered by other authors,¹³ we show that the influence of the holes in the LOPCM line shape is not negligible.

In order to clarify the discussion of the different contributions, provide a unified notation for the different terms, and avoid confusion by some misprints detected in some references, we give a comprehensive outline of the model we have used. The Raman-scattering line shapes are calculated using the fluctuation-dissipation analysis,¹⁹ which for the differential Raman cross section of the LOPCM's yields

$$\frac{\partial^2 \sigma}{\partial \omega \partial \Omega} \propto \Im \left\{ \frac{-1}{\epsilon(\omega)} \left[\frac{\epsilon_\infty}{4\pi} + 2A\chi_I - A^2\chi_I \left(1 + \frac{4\pi}{\epsilon_\infty} \chi_{e-h} \right) \right] \right\}, \quad (3.1)$$

where $\epsilon(\omega) = \epsilon_\infty + 4\pi(\chi_I + \chi_{e-h})$ is the total dielectric function of the electron-hole plasma and

$$A = \frac{\omega_{\text{TO}}^2}{\omega_{\text{LO}}^2 - \omega_{\text{TO}}^2} C. \quad (3.2)$$

C is the Faust-Henry coefficient, and ω_{TO} and ω_{LO} are the zone center transverse and longitudinal optical mode frequencies, respectively. χ_I is the ionic lattice contribution to the susceptibility, which arises from the dipole moments induced by the longitudinal optical modes, and is given by

$$\chi_I = \frac{\epsilon_\infty}{4\pi} \frac{\omega_{\text{LO}}^2 - \omega_{\text{TO}}^2}{\omega_{\text{TO}}^2 - \omega^2 - i\Gamma_I \omega}, \quad (3.3)$$

where Γ_I is a phenomenological ionic damping constant. χ_{e-h} is the electron-hole plasma susceptibility, which contains contributions from both electron and hole intraband transitions as well as heavy-hole–light-hole interband transitions. We assume that the photoexcited carriers are thermalized to a Maxwell-Boltzmann velocity distribution, and that the energy dispersion is parabolic with a carrier effective mass m^* . Considering, as it will be seen below, that the photoexcited carrier densities in our experiments are in the $10^{16}\text{--}10^{17} \text{ cm}^{-3}$ range, the parabolic-band approximation is quite reasonable. Under these assumptions, the intraband frequency-dependent Lindhard dielectric function can be expressed as²¹

$$\chi_{\text{intra}}^{\text{L}}(\omega, q) = -\frac{\epsilon_{\infty}}{8\pi} \frac{1}{(\lambda_D q)^2} \frac{dZ(\eta)}{d\eta}, \quad (3.4)$$

where

$$Z(\eta) = \frac{1}{\sqrt{\pi}} \int_{-\infty}^{+\infty} \frac{e^{-x^2}}{x - \eta} dx \quad (3.5)$$

is the classical-plasma dispersion function, which is related to the complementary error function by²²

$$Z(\eta) = i\sqrt{\pi} e^{-\eta^2} \text{erfc}(-i\eta). \quad (3.6)$$

The parameter η is defined as

$$\eta = \left(\frac{m^*}{2k_B T} \right)^{1/2} \frac{\omega}{q} \quad (3.7)$$

and λ_D is Debye's length given by

$$\lambda_D = \left(\frac{\epsilon_{\infty} k_B T}{4\pi n e^2} \right)^{1/2}, \quad (3.8)$$

where $k_B T$ is the Boltzmann's temperature factor, n is the free-carrier concentration, and e is the electron charge.

Collision damping is included in the intraband susceptibilities using Mermin's prescription,²³

$$\chi_{\text{intra}}(\omega + i\Gamma, q) = \frac{(1 + i\Gamma/\omega) \chi_{\text{intra}}^{\text{L}}(\omega + i\Gamma, q)}{1 + i\Gamma \chi_{\text{intra}}^{\text{L}}(\omega + i\Gamma, q) / [\omega \chi_{\text{intra}}^{\text{L}}(0, q)]}. \quad (3.9)$$

We assume that all free carriers are photoexcited pairs, that is, $n_e = n_{\text{HH}} + n_{\text{LH}}$, and that the density ratio between heavy holes and light holes is given by the equilibrium relation $n_{\text{HH}}/n_{\text{LH}} = (m_{\text{HH}}^*/m_{\text{LH}}^*)^{3/2}$. Under these assumptions, the intraband contributions to the susceptibility given by Eqs. (3.4) and (3.9) are calculated for electrons (χ_e), heavy holes (χ_{HH}), and light holes (χ_{LH}).

The contribution to the susceptibility due to inter-valence-band transitions is evaluated from a Lindhard-type expression weighted by the overlap integrals between the heavy- and light-hole eigenstates. Following the approach of Combescot and Nozières,²⁴ in the Kohn-Luttinger representation for the hole states, the matrix element of the density operator between light- and heavy-hole states of wave vectors \mathbf{k} and $\mathbf{k} + \mathbf{q}$ is given in the small- q limit by

$$|\langle \mathbf{k} | e^{i\mathbf{q} \cdot \mathbf{r}} | \mathbf{k} + \mathbf{q} \rangle|^2 = \frac{3}{4} \left(\frac{q \sin \alpha}{k} \right)^2, \quad (3.10)$$

where α is the angle between \mathbf{k} and \mathbf{q} .

We introduce the reduced mass

$$\mu = \frac{m_{\text{LH}}^* m_{\text{HH}}^*}{m_{\text{HH}}^* - m_{\text{LH}}^*} \quad (3.11)$$

and the transition energy

$$E(k) = \frac{1}{2\mu} \hbar^2 k^2 \equiv \epsilon_{\text{LH}}(k) - \epsilon_{\text{HH}}(k), \quad (3.12)$$

where $\epsilon_{\text{HH}}(k)$ and $\epsilon_{\text{LH}}(k)$ are the kinetic energies of the heavy and light holes in their respective bands.

Then, after integrating over angles, the Lindhard interband susceptibility can be expressed in the $q \rightarrow 0$ limit as an integral over transition energies,

$$\chi_{\text{inter}}(\omega) = -\frac{e^2}{2\pi^2} \int_0^{\infty} dE \left[\hbar \sqrt{\frac{2E}{\mu}} \right]^{-1} [f_{\text{HH}}(E) - f_{\text{LH}}(E)] \times \left[\frac{1}{E + \hbar\omega + i0^+} + \frac{1}{E - \hbar\omega - i0^+} \right], \quad (3.13)$$

where f_{HH} and f_{LH} are the heavy-hole and light-hole Maxwell-Boltzmann distributions.

Using the identity

$$\frac{1}{\omega \pm i\eta} \equiv \wp \left(\frac{1}{\omega} \right) \mp i\pi \delta(\omega) \quad (3.14)$$

the imaginary part of Eq. (3.13) can be written as

$$\Im(\chi_{\text{inter}}) = \frac{1}{4\pi} \sqrt{\frac{2e^4 \mu}{\hbar^3 \omega}} [f_{\text{HH}}(\hbar\omega) - f_{\text{LH}}(\hbar\omega)]. \quad (3.15)$$

Finally, the real part of the susceptibility is evaluated numerically from Eq. (3.15) using the Kramers-Kronig relations.

Damping can be included in the interband term following the outline given in Ref. 25. However, for the low plasma densities involved in our experiments, the effect of interband damping is expected to be small. Therefore, to avoid introducing unnecessary adjustable parameters in the model, we neglect damping in the interband term. To further reduce the number of adjustable parameters, the intraband damping constants are taken to be related by a $\frac{3}{2}$ power of the mass ratio of the different particles. This type of power-law relation between the damping constants and the mass of the particles has been used previously, with exponents $\frac{3}{2} \pm \frac{1}{2}$ (Refs. 9 and 20). In this range, the particular choice of exponent has very little influence on the final values of plasma density obtained from the fits.

The Raman line shape given by Eq. (3.1) is convolved with the instrumental effective slitwidth and fitted to the experimental spectra, with two adjustable parameters, the plasma density n_e and a phenomenological electronic damping constant Γ_e .

To obtain reliable values of the plasma density, particularly at low concentrations where the LOPCM frequency approaches the LO frequency, it is necessary to have accurate determinations of the energy and linewidth of the LO mode. In Table I we list the values of the input parameters that we have used in the model calculations. The phonon energy and linewidth of InP were determined from our own high-resolution measurements at room temperature and at 80 K because the results of the model depend critically on their values. The values for the effective masses, which are the same as those used in Ref. 9, as well as the rest of the parameters were taken from Ref. 26.

In Ref. 20, the susceptibility terms corresponding to heavy holes, light holes, and interband heavy-hole-light-

TABLE I. List of parameters used in the calculations. The values were taken from Ref. 26, except for ω_{LO} , ω_{TO} , and Γ_{LO} , which were obtained from our own measurements. The values inside parentheses correspond to 80 K. The values of Γ_{LO} have been corrected for experimental resolution.

Symbol	Description	Value
m_e^*	Electron effective mass	$0.079 m_0$
m_{HH}^*	Heavy-hole effective mass	$0.45 m_0$
m_{LH}^*	Light-hole effective mass	$0.12 m_0$
C	Faust-Henry coefficient	-0.14
ϵ_∞	High-frequency dielectric constant	9.61
ω_{LO}	LO phonon frequency	343.5 cm^{-1} (346.8 cm^{-1})
ω_{TO}	TO phonon frequency	303.8 cm^{-1} (306.4 cm^{-1})
Γ_{LO}	LO linewidth	1.2 cm^{-1} (0.45 cm^{-1})

hole transitions were separately incorporated to the LOPCM line-shape model for heavily doped ($5 \times 10^{18} \text{ cm}^{-3}$) p -GaAs, and the importance of including the light-hole and interband terms in addition to the heavy-hole term was clearly demonstrated. In the present work, we show the influence of the different terms contributing to the susceptibility for the case of a photoexcited electron-hole plasma. This system differs substantially from that reported in Ref. 20 in that, first, the electronic contribution has to be included, and, second, the input parameters of the model correspond to a much lower density plasma. Consequently, the individual contributions to the susceptibility are significantly different.

To evaluate the effect of including the hole contributions in the electron-hole plasma model, we compare in Fig. 1 the L^+ line shape calculated using the full model with the results of calculations in which different hole contributions have been neglected. In contrast to the high values of charge density used in Ref. 20, we have carried out these calculations for $n_e = 5 \times 10^{17} \text{ cm}^{-3}$ and $\Gamma_e = 100 \text{ cm}^{-1}$, which are values of plasma density and electronic damping representative of photoexcited plasma in semiconducting InP (see Sec. IV).

As can be seen in Fig. 1, neglecting all the hole terms leads to a narrower and more symmetric L^+ line shape (dashed-dotted line). The addition of the intraband heavy-hole contribution does not change substantially the line

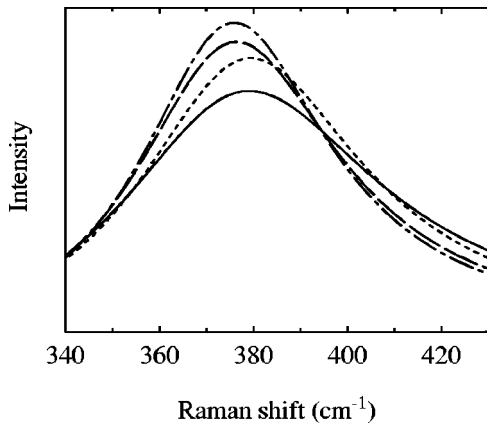


FIG. 1. LOPCM line shapes calculated for $n_e = 5 \times 10^{17} \text{ cm}^{-3}$ and $\Gamma_e = 100 \text{ cm}^{-1}$ using the model described in Sec. III, where the plasma susceptibility has been set to $\chi = \chi_e$ (dashed-dotted line), $\chi = \chi_e + \chi_{\text{HH}}$ (dashed line), $\chi = \chi_e + \chi_{\text{HH}} + \chi_{\text{LH}}$ (dotted line), and $\chi = \chi_e + \chi_{\text{HH}} + \chi_{\text{LH}} + \chi_{\text{inter}}$ (solid line).

shape (dashed line), mainly because of the overdamped nature of the heavy holes for the parameters used in the calculation. When the less-damped light holes are included in the model, the L^+ peak shifts to higher energies and broadens, reflecting the increase of charge and damping in the plasma (dotted line). Finally, including the contribution of heavy-hole–light-hole interband transitions to the susceptibility introduces an additional intrinsic source of damping in the electron-hole plasma, which is reflected in a broader, more asymmetric line shape (solid line) with a tail towards its high-energy side. This type of line shape provides the best fits to the experimental Raman spectra (see Sec. IV). The results of the full model for the parameters used to obtain the curves shown in Fig. 1 yield an L^+ frequency about 3 cm^{-1} higher than the value obtained when the holes are completely neglected. Typically, plasma densities about 20% higher are obtained if the fits are carried out using a model including only electrons instead of the full model in which the different hole contributions are also taken into account.

IV. PHOTOEXCITED PLASMA IN SEMICONDUCTING InP

Figure 2 shows polarized Raman spectra of semiconducting InP excited with different laser powers in the 3–55 mW range, corresponding to laser-power densities between 7 and 133 W cm^{-2} . For higher incident laser power the higher damping in the plasma gives rise to very broad structures for which the fitted parameters would have a larger uncertainty.

The Raman measurements were performed in $z(x,y)\bar{z}$ scattering geometry, where both LO-phonon and LOPCM Raman scattering are allowed via deformation potential mechanism.²⁷ Two peaks can be observed in the spectra of semiconducting InP shown in Fig. 2. The frequency of the low-energy peak, 343.5 cm^{-1} at room temperature and 346.8 cm^{-1} at 80 K, does not change with the exciting laser power. This peak is due to the unscreened LO modes of the surface depletion zone. We find a LO frequency lower than values previously reported, which range from 344.5 (Ref. 28) to 348.5 cm^{-1} (Ref. 29) at room temperature. We shall discuss below possible reasons for these discrepancies. The high-energy peak of the spectra displayed in Fig. 2 exhibits an absolute dependence on the laser power, and we assign it to the L^+ branch of the LOPCM's. As can be seen in Fig. 2(a), the LO and L^+ peaks can be resolved at room tempera-

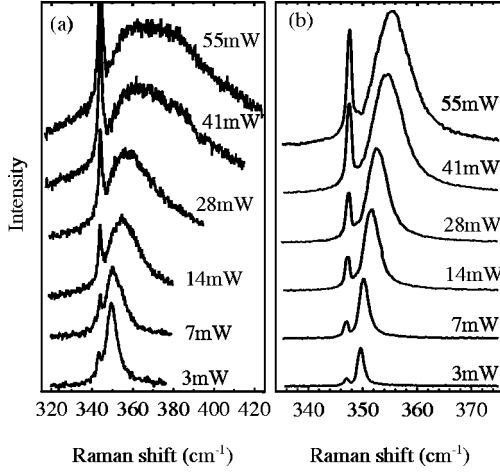


FIG. 2. (a) Room-temperature Raman spectra of semiconducting InP at different incident laser powers, showing the shift to higher energies of the L^+ coupled modes with the excitation power. (b) As in (a), at 80 K. Note the different scale on the frequency axes of these plots. The spectra were recorded in the $z(x,y)\bar{z}$ scattering geometry.

ture for an incident laser power of 3 mW. In Fig. 2(b) we show the Raman spectra of semiconducting InP recorded at 80 K. The separation between the LO and L^+ peaks is improved at low temperature because the linewidths of both peaks are notably reduced. In measurements at 80 K, we have been able to resolve the LO and L^+ peaks even for a laser-power density as low as 0.8 W cm^{-2} .

In Table II we compare our results with previously reported data¹¹⁻¹³ on electron-hole plasma generated by cw-laser excitation in semiconducting InP. We have included the lowest and highest power densities reported in each article. Whereas at room temperature we have been able to resolve the L^+ peak of the photoexcited plasma for power densities as low as 7 W cm^{-2} , power densities above 200 W cm^{-2}

were necessary to resolve the L^+ peak at room temperature in previous works.^{11,12} As can be seen in Table II, the largest LO- L^+ splittings reported in Refs. 11 and 12 are similar to ours, but were obtained for power densities one order of magnitude larger. Several factors may contribute to these differences. The accuracy in the determination of the spot size, which can lead to large variations in the estimated laser-power density, and the low resolution used in some experiments may play an important role in the observed discrepancies. In addition, the data from Ref. 11 correspond to a lightly doped InP sample, and the presence of the free-electron plasma may have obscured the observation of the photoexcited plasma. Also, the recombination rate of the photoexcited electron-hole pairs may be different in this sample due to the presence of dopant impurities. Some differences with the results reported in Ref. 13 could be expected from the fact that those experiments were carried out near the $E_0 + \Delta_0$ resonance, where the absorption coefficient of InP is significantly lower than for the wavelength we have used.³⁰ Nevertheless, the observation in that work of a single peak, assigned to the L^+ mode, in the $z(x,y)\bar{z}$ scattering geometry, in spite of the high power densities used, is a surprising result, as LO-phonon Raman scattering is allowed in this geometry near the $E_0 + \Delta_0$ resonance via deformation potential mechanism.³¹ Moreover, this peak exhibits a frequency shift of only 0.2 cm^{-1} when the laser-power density is increased by a factor of 4, while its shape and width are very similar to that of the LO peak seen in the $z(x,x)\bar{z}$ spectrum. Surprisingly, only a single peak can be seen in this spectrum, in spite of the fact that Raman scattering by both LO and L^+ modes is allowed in this geometry near the $E_0 + \Delta_0$ resonance via impurity-induced Fröhlich interaction.^{27,31} Considering the very small shift with increasing laser power of the peak observed in the $z(x,y)\bar{z}$ spectra, the presence of only one peak in each configuration, and the very similar width of the peaks seen in both configu-

TABLE II. Comparison of our results with previously reported data on cw-laser photoexcited plasma in semiconducting InP. We have included the lowest and the highest power densities reported in each article. The results from Ref. 11 displayed in the table correspond to the least doped sample ($n = 9 \times 10^{16} \text{ cm}^{-3}$). The splitting and the plasma density quoted for this sample correspond to the shift of the L^+ peak and the photoexcited excess-carrier density, respectively.

Temperature (K)	Power (mW)	Power density (W cm^{-2})	L^+ -LO splitting (cm^{-1})	Plasma density (cm^{-3})	Ref.
RT	3	7	6.3	9×10^{16}	a
RT	55	133	24.0	5.2×10^{17}	a
80	3	7	2.6	4×10^{16}	a
80	55	133	7.8	1.4×10^{17}	a
RT		100	0	0	b
RT		1200	22	2.8×10^{17}	b
RT		116	0		c
RT		928	20		c
10		40	0.4	1.5×10^{16}	d
10		1360	0.6	3.3×10^{16}	d

^aPresent work.

^bReference 11.

^cReference 12.

^dReference 13.

rations, the possibility that the peak observed in the $z(x,y)\bar{z}$ configuration actually corresponds to the LO mode should not be ruled out.

The model developed in Sec. III, which we use to determine the density of photoexcited plasma from the Raman spectra, assumes a uniform plasma and therefore it yields reliable fits of the LOPCM Raman line shape with a single value for the plasma density and for the electronic damping provided that the photoexcited plasma can be considered homogeneous in the region probed by Raman scattering.

Young *et al.*¹⁵ evaluated the homogeneity of the photoexcited carriers in InP for time-resolved Raman-scattering experiments in which the probing light is delayed a few picoseconds from the exciting pulse. These authors already found a highly homogeneous distribution of the photoexcited carriers in InP over the region probed by the laser, in contrast with the highly inhomogeneous profiles generated in GaAs. In the present paper, we evaluate the homogeneity of the photoexcited plasma in InP under the experimental conditions used in our measurements, which have substantial differences in relation to those of Ref. 15. First, the Raman-scattering experiments were carried out in steady-state conditions under continuous excitation. Therefore, the bulk recombination, which was not taken into account in Ref. 15 because the bulk recombination lifetime is very large in relation to the delay time, must be included in the profile calculations. Second, an unusually high value of SRV for InP was used in Ref. 15. And finally, the penetration depth for the laser wavelength used in our experiments is lower than that of Ref. 15. Taking into account these differences, and assuming also a punctual laser beam, we have calculated the depth profile of the photoexcited carriers for steady-state conditions by solving a simple one-dimensional diffusion equation. A density-independent ambipolar diffusion coefficient of $4.5 \text{ cm}^2/\text{s}$ (Ref. 18) was used in the calculations. The recombination lifetime τ is taken inversely proportional to the carrier density, $\tau = 1/Bn_e$,³² with B the coefficient for the radiative transition probability, which was determined to be $3.33 \times 10^{-10} \text{ cm}^3 \text{ s}^{-1}$ for InP.³² In the range of SRV's reported in the literature,¹⁶⁻¹⁸ the calculated carrier profile is not sensitive to the particular choice of SRV. In our calculation we have used the value of 100 cm s^{-1} .¹⁶ The absorption coefficient of InP at 528.7 nm was taken as $1.02 \times 10^5 \text{ cm}^{-1}$.³⁰

In Fig. 3 we plot the photoexcited-charge profiles for the first 300 nm from the surface obtained by numerical integration of the diffusion equation. We have calculated the profile for a charge density of $5 \times 10^{17} \text{ cm}^{-3}$ at the surface, which is approximately the highest plasma density observed in our experiments. The depth profiles were normalized to the charge density at the surface. Considering the absorption coefficient of InP for the wavelength used in our experiments, only about 10% of the initial intensity of the laser beam is acting as probing light at a depth of 110 nm. Then, according to the results shown in Fig. 3, the inhomogeneity of the plasma density in the region probed by the laser is less than 2%. Also displayed in Fig. 3 is the depth profile for a charge at the surface one order of magnitude lower, showing that the relative variation of the plasma density decreases for lower densities, and is less than 0.5% for $5 \times 10^{16} \text{ cm}^{-3}$ within 110 nm from the surface. So, according to these results, over

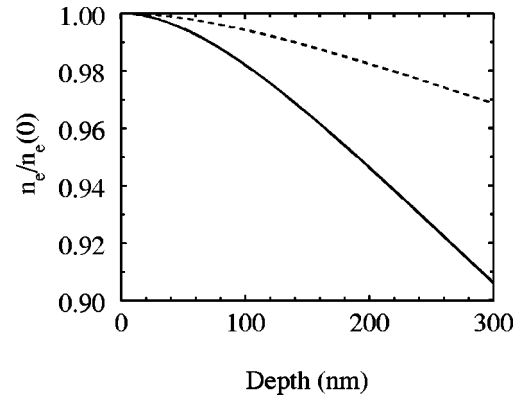


FIG. 3. Relative variation of the photoexcited plasma density with depth for InP under continuous excitation conditions. The curves, normalized to the plasma density at the surface $n_e(0)$, have been calculated from a one-dimensional diffusion equation for $n_e(0)$ values of $5 \times 10^{17} \text{ cm}^{-3}$ (solid line) and $5 \times 10^{16} \text{ cm}^{-3}$ (dotted line).

the region probed by the laser the homogeneity of the photoexcited carriers in InP for steady-state conditions is even higher than that reported in Ref. 15.

Obviously, this one-dimensional diffusion model is too simple to yield reliable absolute values for the photoexcited plasma density. We use it only to estimate the relative variations of the charge density within the range of depths probed by the laser.

Lateral inhomogeneity in the photoexcited plasma may arise from the Gaussian intensity profile of the laser beam. Sampling regions with different plasma densities could give rise to shifts and broadenings of the LOPCM peak, as the energy of the coupled modes depends on the plasma density. To model the influence of lateral inhomogeneity on the LOPCM spectra, we have generated a laterally averaged line shape (LAL), which incorporates the effects of the Gaussian intensity profile of the laser beam in the following way. First, we assume a linear dependence between the photoexcited charge density and the intensity of the laser light, which is consistent with the results shown in Fig. 4, and hence the photoexcited charge is also assumed to have a Gaussian profile. Then, the individual LOPCM contributions to the LAL, corresponding to the different plasma densities across the photoexcited Gaussian profile, are calculated using the model described in Sec. III. The electronic damping coefficient used to calculate the LOPCM line shape for each plasma density is obtained from the results shown in Fig. 4. Finally, the LAL is constructed as the weighted average of the LOPCM line shapes over the slit width of the spectrometer, taking into account the Gaussian profile of the laser intensity.

To evaluate the accuracy of the plasma density and damping parameter values obtained by fitting the model of Sec. III, we fitted this single-LOPCM model to the LAL's described above, which were generated for plasma densities in the range of those found in the experiments on semiconducting InP. It was found that the plasma-density value obtained from the single-LOPCM fit is within 3% of the average charge density in the Gaussian density distribution used to generate the LAL. On the other hand, the damping parameter obtained from the single-LOPCM fit is only about 4 cm^{-1}

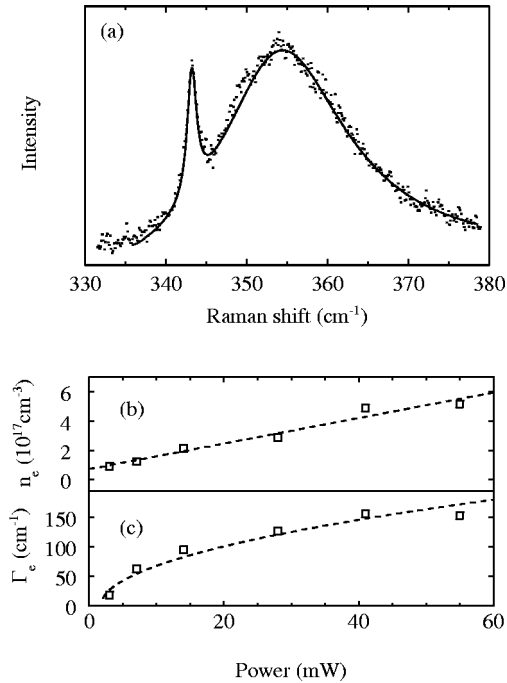


FIG. 4. (a) Line-shape fit (solid line) to the experimental data (dots) corresponding to semiconducting InP with an incident laser power of 14 mW. The line shape was calculated using the Lindhard-Mermin dielectric function as explained in Sec. III. The LO mode arising from the surface depletion zone was fitted with a Lorentzian line shape. (b) Density of photoexcited plasma as a function of laser power in semiconducting InP at room temperature as determined from the fit. (c) Values of electronic damping for the photoexcited plasma at different laser powers.

larger than the damping coefficient that is associated with the corresponding charge density according to the relationship between Γ_e and n_e shown Fig. 4, which was assumed in the generation of the LAL. Therefore, the laser intensity profile has only a small effect on the LOPCM line shapes and it will not be considered in the analysis of the LOPCM Raman spectra.

The profiles shown in Fig. 3 do not include the surface depletion zone. We can make a rough estimation of the surface depletion depth applying the simple model used by Pinczuk *et al.*³³ to determine depletion depths in doped InP. Using the air/*n*-type InP band-bending value of 0.2 eV reported by these authors,³³ we find for a carrier density of 5×10^{17} cm⁻³ a depletion depth of 17 nm. According to Fig. 3, such a narrow depletion zone has no influence on the homogeneity of the remaining region probed by the laser.

All the above considerations about the inhomogeneity of the photoexcited plasma and its possible effects on the analysis of the photoexcited charge indicate that, for InP under cw excitation, the photoexcited plasma density and damping coefficient can be adequately determined from Raman spectra using the theory of Sec. III.

Given that for the plasma densities involved in our experiments the LO- L^+ splitting is not very large, accurate values of the LO frequency are essential to obtain meaningful results from the model. Values for the LO frequency and linewidth quoted in the literature are usually too large,^{9,28,29} probably due to the overlapping of the unresolved L^+ peak with the LO mode because of the low experimental resolu-

tion used. We have determined the LO frequency and linewidth at room temperature and at 80 K from high-resolution (effective slitwidth ≈ 0.7 cm⁻¹) Raman spectra in which the LO and the L^+ modes were well resolved. The values are listed in Table I, where the linewidths have been corrected for instrumental broadening.

In Fig. 4 we plot the results of the fitting procedure. As can be seen in Fig. 4(a), where we display the model line-shape fit to the room-temperature Raman spectrum obtained with a laser power of 14 mW, very good fits to the experimental data can be obtained. In Fig. 4(b) we plot the photoexcited-plasma density as obtained from the line-shape fits versus the incident laser power. In the laser-power range studied, the density of the photoexcited plasma shows an almost linear increase with the incident power, from 9×10^{16} cm⁻³ for 3 mW to 5.2×10^{17} cm⁻³ for 55-mW excitation at room temperature. At 80 K, the photogenerated plasma density takes values from 5.6×10^{16} cm⁻³ for 3 mW to 1.4×10^{17} cm⁻³ for 55 mW. Both the density of photoexcited plasma and its rate of change with laser power are lower at 80 K. As the temperature is lowered from 300 to 80 K, both the SRV and the ambipolar diffusion constant increase,^{34,35} which may play an important role in the reduction of plasma density detected in Raman-scattering experiments. Further investigations should be carried out to clarify this point.

The values of the phenomenological damping parameter obtained from the fits are plotted in Fig. 4(c). The damping increases with the exciting laser power, from about 20 cm⁻¹ for 3 mW to about 150 cm⁻¹ for 55-mW excitation, reflecting the increase of the electron-hole plasma density, and hence, of the scattering rate in the photoexcited plasma. At low exciting powers the L^+ peak narrows considerably, particularly in the low-temperature measurements. The full width at half maximum of the L^+ peak obtained at 80 K and 3-mW excitation after correction for the experimental broadening is just 1.4 cm⁻¹, only about three times the linewidth of the LO mode. For this spectrum, we calculate a plasma density of $\approx 4 \times 10^{16}$ cm⁻³ and a damping parameter of ≈ 4 cm⁻¹. Such small damping parameters are not uncommon in photoexcited plasmas. Pinczuk *et al.*¹⁴ have pointed out that photoexcited electrons have unusually long relaxation times in GaAs, about ten times longer than in equivalently doped *n*-type GaAs, and have reported values of damping below 5 cm⁻¹ for capped GaAs at low temperature.

We have shown that, even for low incident laser powers, the density of photoexcited plasma in semiconducting InP can be high enough to be detected by means of Raman spectroscopy. L^+ modes can be observed by this technique at room temperature for an incident laser power as low as 3 mW. This may have a significant influence on experiments made on InP under cw-laser illumination and should be taken into account in future experiments.

V. PHOTOEXCITED PLASMA IN SEMI-INSULATING InP

To our knowledge, no experimental evidence of coupled L^+ modes has been reported so far for semi-insulating InP under cw-laser excitation. In a previous work¹² a broadening of the LO peak was observed as the laser power was in-

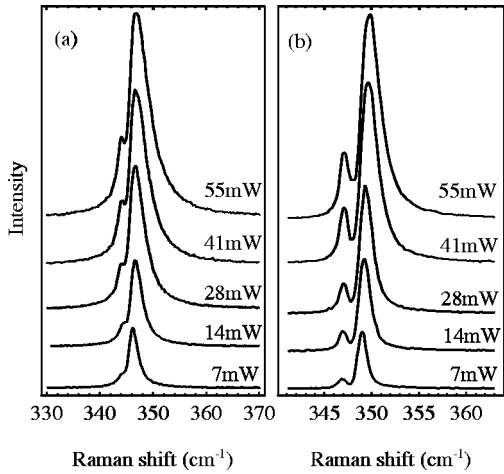


FIG. 5. (a) Room-temperature Raman spectra of semi-insulating InP at different incident laser powers. (b) As in (a) at 80 K. Note the different scale on the frequency axes of these plots. The spectra were recorded in the $z(x,y)\bar{z}$ scattering geometry.

creased, but the L^+ and LO peaks could not be resolved even for laser-power densities close to 2000 W cm^{-2} .

In Fig. 5(a) we show the room-temperature Raman spectra of semi-insulating InP for laser powers from 7 to 55 mW. Whereas for low laser powers only a shoulder can be seen on the low-energy side of the main Raman peak, two peaks are clearly resolved for higher laser powers. As already discussed for semiconducting InP, the low energy peak is due to the unscreened LO modes from the surface depletion zone, while the high-energy peak corresponds to the L^+ coupled modes. To reduce the linewidths and better resolve these two peaks, we carried out Raman measurements at 80 K in the same power range. Figure 5(b) shows the Raman spectra of semi-insulating InP at 80 K, where LO and L^+ modes are clearly resolved even for the lowest laser power.

Comparing Figs. 2 and 5 we can see that, for the same laser power, the LO- L^+ shift is much larger in semiconducting InP, indicating a significantly higher plasma density. Semi-insulating InP, with resistivities of the order of $10^7 \Omega \text{ cm}$, is obtained by doping the InP crystal with Fe during the growth. The Fe impurity occupies In sites substitutionally and introduces a deep level that compensates residual shallow donors, thereby forming semi-insulating material.³⁶ Semi-insulating InP contains neutral (Fe^{3+}) and singly ionized (Fe^{2+}) acceptor states that have energies close to the middle of the gap,^{37,38} and therefore the Fe centers in InP act as efficient recombination centers for the photoexcited electron-hole pairs. As a result of the different electron-hole recombination kinetics, the density of photoexcited plasma for a given laser power is substantially reduced in semi-insulating InP:Fe.

We have used the model discussed in Sec. III to fit the measured Raman spectra in order to determine the photoexcited-plasma density in semi-insulating InP. Figure 6(a) shows the theoretical line shape (solid line) fitted to the room-temperature Raman spectrum (dots) obtained with a laser power of 14 mW. Reasonably good fits are obtained, although the experimental spectra show an asymmetric high-energy tail that is not accurately reproduced by the model. In Fig. 6(b) we plot the photoexcited-plasma density versus la-

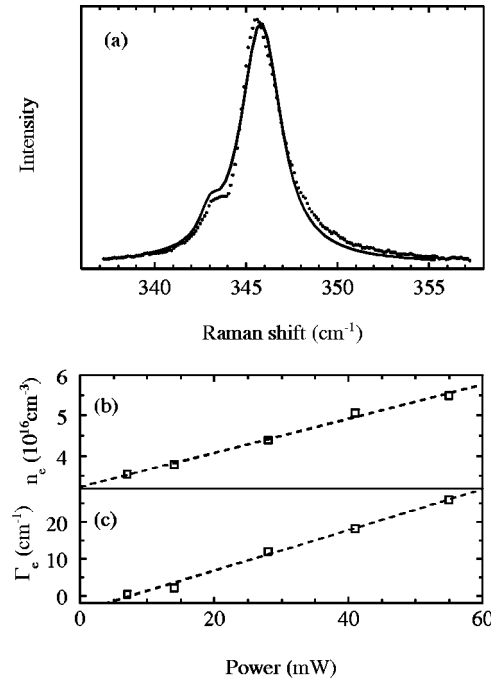


FIG. 6. (a) Line-shape fit (solid line) to the experimental data (dots) corresponding to semi-insulating InP with an incident laser power of 14 mW. The line shape was calculated using the Lindhard-Mermin dielectric function as explained in Sec. III. The LO mode arising from the surface depletion zone was fitted with a Lorentzian line shape. (b) Density of photoexcited plasma as a function of laser power in semi-insulating InP at room temperature as determined from the fit. (c) Values of electronic damping for the photoexcited plasma at different laser powers.

ser power at room temperature as obtained from the fitting procedure. The photoexcited-plasma density obtained from the fits as well as its rate of change with laser power are typically one order of magnitude smaller in semi-insulating InP in relation to semiconducting InP. In both cases the photoexcited carrier density increases almost linearly with laser power in the range of laser powers studied. In contrast with semiconducting InP discussed in Sec. IV, where a significant decrease of the photoexcited charge was observed at 80 K, the photoexcited-plasma density in semi-insulating InP at 80 K is roughly the same as at room temperature. In semi-insulating InP, lower capture rates at the Fe centers at 80 K (Ref. 37) could explain an increase of photogenerated charge at low temperature that would counterbalance the higher surface recombination and carrier diffusivity at low temperature discussed in Sec. IV.

We compare now our results with the photoexcited-plasma densities determined from time-resolved Raman-scattering experiments on semi-insulating InP.⁹ The largest Raman shift for the L^+ peak found in that work was 364.7 cm^{-1} at 28.6-ps delay, much higher than the value we have observed in our semi-insulating samples at 55-mW laser excitation. This is not surprising, since in those experiments the electron-hole plasma was excited using laser pulses with an average power of 480 mW. The photoexcited-plasma density estimated in Ref. 9 from that Raman spectrum was $4.8 \times 10^{17} \text{ cm}^{-3}$. Although this value is close to those we find for semiconducting InP for similar L^+ peak frequencies, we point out a significant difference between the analysis used

to extract the plasma density in that paper and the approach we have followed here. In fact, we have two adjustable parameters in the model, namely, the photoexcited plasma density and a phenomenological electronic damping constant. By contrast, in Ref. 9 all the spectra obtained for a given pump-beam fluence were fitted with the same damping parameter, which was taken as 280 cm^{-1} , regardless of the fact that a significant variation of the plasma density for different delay times was observed. As the plasma density and hence the scattering rates increase, the damping parameter is also expected to increase. In fact, as can be seen in Figs. 4(c) and 6(c), our results show a sizable increase of the electronic damping parameter in the range of power densities studied. However, we have obtained damping values significantly lower than the value used in Ref. 9, even for comparable plasma densities. Too large damping parameters in the model yield broader L^+ line shapes shifted to lower frequencies, and consequently, a larger plasma-density parameter has to be used in the model to obtain good fits to the experimental spectra. On the other hand, we note that in Ref. 9 a value of 345.5 cm^{-1} for the LO-phonon frequency and an ionic damping constant of 3 cm^{-1} were used in the calculations. As we discuss below, these values of ω_{LO} and Γ_{LO} , taken from previously reported measurements, are probably too large. Actually, the sharp peak reported as of unclear origin in Ref. 9 slightly below the LO energy, whose frequency is in good agreement with the LO frequency of 343.5 cm^{-1} determined in the present work, could be due to the unscreened LO mode of the surface depletion zone. The use of a too large value for the LO frequency in the model underestimates the plasma density because it reduces the LO- L^+ splitting. This roughly compensates the overestimation of the plasma density due to the high damping value, and the plasma densities reported in Ref. 9 are similar to the values we have found for similar LO- L^+ splittings.

As mentioned above, there is a wide range of reported values for the energy of the LO mode of InP, ranging from 344.5 cm^{-1} (Ref. 28) to 348.5 cm^{-1} (Ref. 29) at room temperature. Differences in experimental calibration should account only for a small proportion of this dispersion of LO-frequency values. However, the presence of photogenerated carriers in InP, even at small laser powers, can give rise to changes in the Raman spectra that explain the dispersion of LO-mode energies found for this compound in the literature. Unless the Raman measurements are performed with high resolution, the peaks corresponding to the LO mode and to the photoexcited L^+ coupled mode cannot be resolved, and a single peak is observed in the LO-mode energy region. The frequency and linewidth of this peak are mainly determined by the L^+ mode, which overlaps the actual LO mode. As the L^+ peak is centered at higher energy and has a larger linewidth than the LO peak, a wide range of higher ‘‘LO’’ frequencies and linewidths can be found in the literature depending on the laser-power density used to excite the Raman spectra and the characteristics of the InP sample. This fact should be taken into account when accurate measurements of

the LO mode of InP are required, as for instance, in the determination of the strain in InP-based superlattices by means of the LO-mode strain-induced shift.³⁹

VI. CONCLUSIONS

We have presented a study of photoexcited coupled LO-plasmon modes in semiconducting and semi-insulating InP under cw-laser excitation. For the first time, to our knowledge, the LO and L^+ peaks have been resolved in semi-insulating InP using cw-laser power excitation, thereby providing evidence of Raman scattering by photoexcited charge in semi-insulating InP at power densities commonly used in Raman-scattering experiments. In semiconducting InP, the LO and L^+ peaks could be resolved for power densities much lower than previously reported.

Both in semiconducting and semi-insulating InP, the photogenerated plasma density is high enough to be detected by Raman measurements even at low laser excitation level. The accuracy of previous determinations of the energy and linewidth of the LO mode may have been affected by the presence of photoexcited charge. Since the L^+ and LO peaks overlap, a single peak mainly due to the L^+ coupled mode is detected when Raman measurements are performed with low resolution, and therefore too large values of the LO energy and linewidth are obtained. This should be taken into account when accurate measurements of the LO-mode energy and linewidth are required.

The photoexcited-plasma density has been determined from Raman spectra by fitting a line-shape model based on a Lindhard-Mermin dielectric function that takes into account interband hole transitions as well as electron and heavy- and light-hole intraband transitions. It has been shown that to obtain good fits to the experimental spectra and accurate values of the photoexcited-plasma density, the hole contribution cannot be neglected. Two adjustable parameters, namely the plasma density and a phenomenological electronic damping constant, are required to obtain good fits to the Raman spectra. In the range of laser powers studied, it was found that the photoexcited plasma density increases almost linearly with the incident laser power for both semiconducting and semi-insulating InP. Photoexcited-plasma densities up to $\approx 5 \times 10^{17} \text{ cm}^{-3}$ were found in semiconducting InP at room temperature for laser powers up to 55 mW, while for the same range of laser powers the plasma densities in semi-insulating InP were about one order of magnitude lower, due to the efficient recombination of photoexcited carriers at the Fe centers.

ACKNOWLEDGMENTS

We are grateful to G. González-Díaz for supplying the InP samples and for useful comments. The authors would also like to acknowledge the Spanish Ministerio de Educación y Ciencia for financial support. One of us (J.I.) acknowledges CSIC for financial support.

- ¹T. Kawakami and M. Okamura, *Electron. Lett.* **15**, 502 (1979).
- ²B. K. Ridley, *J. Appl. Phys.* **48**, 754 (1977).
- ³K. Kamimura, T. Suzuki, and A. Kunioka, *Appl. Phys. Lett.* **38**, 259 (1981).
- ⁴J. E. Hurwitz and J. J. Hsieh, *Appl. Phys. Lett.* **32**, 487 (1978).
- ⁵T. P. Pearsall and R. W. Hopson, Jr., *J. Electron. Mater.* **7**, 133 (1978).
- ⁶J. E. Kardontchik and E. Cohen, *Phys. Rev. Lett.* **42**, 669 (1979).
- ⁷G. Abstreiter, M. Cardona, and A. Pinczuk, in *Light Scattering in Solids IV*, edited by M. Cardona and G. Güntherodt, Topics in Applied Physics Vol. 54 (Springer-Verlag, Berlin, 1984).
- ⁸A. R. B. de Castro and R. S. Turtelli, *Solid State Commun.* **47**, 475 (1983).
- ⁹J. F. Young and K. Wan, *Phys. Rev. B* **35**, 2544 (1987).
- ¹⁰K. T. Tsen, G. Halama, O. F. Sankey, S. C. Y. Tsen, and H. Morkoc, *Phys. Rev. B* **40**, 8103 (1989).
- ¹¹T. Nakamura and T. Katoda, *J. Appl. Phys.* **55**, 3064 (1984).
- ¹²B. Boudart, B. Mari, and B. Prevot, *Mater. Sci. Eng., B* **20**, 109 (1993).
- ¹³E. T. M. Kernohan, R. T. Phillips, B. H. Bairamov, D. A. Ritchie, and M. Y. Simmons, *Solid State Commun.* **100**, 263 (1996).
- ¹⁴A. Pinczuk, J. Shah, and P. A. Wolff, *Phys. Rev. Lett.* **47**, 1487 (1981).
- ¹⁵J. F. Young, K. Wan, A. J. Spring Thorpe, and P. Mandeville, *Phys. Rev. B* **36**, 1316 (1987).
- ¹⁶V. Diadiuk, S. H. Groves, C. A. Armiento, and C. E. Hurwitz, *Appl. Phys. Lett.* **42**, 892 (1983).
- ¹⁷H. C. Casey, Jr. and E. Buehler, *Appl. Phys. Lett.* **30**, 247 (1977).
- ¹⁸Y. Rosenwaks, Y. Shapira, and D. Huppert, *Appl. Phys. Lett.* **57**, 2552 (1990).
- ¹⁹D. T. Hon and W. L. Faust, *Appl. Phys.* **1**, 241 (1973).
- ²⁰K. Wan and J. F. Young, *Phys. Rev. B* **41**, 10 772 (1990).
- ²¹P. M. Platzman and P. A. Wolff, *Solid State Physics* (Academic Press, New York, 1973), Suppl. 13.
- ²²M. Abramowitz and I. Stegun, *Handbook of Mathematical Functions*, Applied Mathematics Series Vol. 55 (Dover, New York, 1968).
- ²³N. D. Mermin, *Phys. Rev. B* **1**, 2362 (1970).
- ²⁴M. Combescot and P. Nozières, *Solid State Commun.* **10**, 301 (1972).
- ²⁵J. Monecke, *Phys. Status Solidi B* **121**, 329 (1984).
- ²⁶O. Madelung, W. von der Osten, and U. Rössler, in *Numerical Data and Functional Relationships in Science and Technology*, edited by O. Madelung, Landolt-Börnstein, New Series, Group III, Vol. 17a (Springer-Verlag, Berlin, 1982).
- ²⁷D. Olego and M. Cardona, *Phys. Rev. B* **24**, 7217 (1981).
- ²⁸R. Trommer, H. Müller, M. Cardona, and P. Vogl, *Phys. Rev. B* **21**, 4869 (1980).
- ²⁹E. Bedel, G. Landa, R. Carles, J. P. Redoulès, and J. B. Renucci, *J. Phys. C* **19**, 1471 (1986).
- ³⁰D. E. Aspnes and A. A. Studna, *Phys. Rev. B* **27**, 985 (1983).
- ³¹W. Kauschke and M. Cardona, *Phys. Rev. B* **33**, 5473 (1986).
- ³²R. K. Ahrenkiel, D. J. Dunlavy, and T. Hanak, *J. Appl. Phys.* **64**, 1916 (1988).
- ³³A. Pinczuk, A. A. Ballman, R. E. Nahory, M. A. Pollack, and J. M. Worlok, *J. Vac. Sci. Technol.* **16**, 1168 (1979).
- ³⁴B. M. Keyes, D. J. Dunlavy, R. K. Ahrenkiel, G. Shaw, G. P. Summers, N. Tzafaras, and C. Lentz, *J. Appl. Phys.* **75**, 4249 (1994).
- ³⁵J. F. Young and H. M. van Driel, *Phys. Rev. B* **26**, 2147 (1982).
- ³⁶W. H. Koschel, U. Kaufmann, and S. G. Bishop, *Solid State Commun.* **21**, 1069 (1977).
- ³⁷P. B. Klein, J. E. Furneaux, and R. L. Henry, *Phys. Rev. B* **29**, 1947 (1984).
- ³⁸L. Eaves, A. W. Smith, P. J. Williams, B. Cockayne, and W. R. MacEwan, *J. Phys. C* **14**, 5063 (1981).
- ³⁹B. Jusserand and M. Cardona, in *Light Scattering in Solids V*, edited by M. Cardona and G. Güntherodt, Topics in Applied Physics Vol. 66 (Springer-Verlag, Berlin, 1989).